Photoinduced electron transfer in mixed-valence compounds: Beyond the golden rule regime

D. G. Evans
Department of Chemistry, University of New Mexico, Albuquerque, New Mexico 87131

A. Nitzan
Department of Chemistry, Tel Aviv University, Tel Aviv, Israel 69978

M. A. Ratner
Department of Chemistry, Northwestern University, Evanston, Illinois 60208

(Received 14 July 1997; accepted 17 December 1997)

The short-time charge transfer evolution following photoexcitation in mixed valence compounds is studied using path integral calculations. Due to the large nonadiabatic coupling, path integral calculations using direct path summation techniques are inadequate, and charge transfer dynamics can only be computed using a transfer matrix technique developed by Makri and Makarov. The resulting relaxation is considerably slower than that predicted by low-order perturbation theory. The effects of the solvent on the decay process, and the validity of the golden rule to predict the dynamics of the decay process are investigated. The effects of preparing an initial state that is not a rovibrational state of the acceptor potential energy surface is also examined. These exact calculations show that the large electronic mixing gives rise to very fast oscillations in the electronic state population as the wave function oscillates coherently between the donor and acceptor. This is followed by a slower relaxation induced by the coupling to the dissipative solvent modes, which occurs on time scales $\leqslant 100$ fs. This information provides insight into the mechanism for oscillations observed in time-resolved transient spectra of these compounds, and suggests substantial limitations of the golden rule picture. © *1998 American Institute of Physics.* [S0021-9606(98)50412-6]

I. INTRODUCTION

Current experiments on electron transfer processes in photoexcited mixed valence compounds[1–5] have provided a wealth of experimental data on condensed phase electron transfer processes. These short-time pulse experiments show a variety of intricate behaviors and a knowledge of the time scales of all the physical processes involved is essential to understanding these details.[3–5] In particular, the back electron transfer experiments involve excitation of an initially equilibrated molecule to a charge transfer state where the nuclear geometry is far from its equilibrium configuration. The relative time scales of the back electron transfer reaction and of the solvent response must be known in order to understand if the oscillations observed on the time scale from dozens to hundreds of femtoseconds are caused by intramolecular vibrational or electronic coherences associated with electron transfer, or rather by reorganization of the solvent structure.[2]

As illustrated in Fig. 1, photoexcitation experiments in mixed valence species involve two processes: initial photoexcitation from the initial (hereafter called donor) electronic surface onto the final (hereafter called acceptor) electronic surface, followed by a slower back electron transfer process from this acceptor surface to the donor electronic surface:[2,5,6]

$$DA \xrightarrow{\hbar\omega} D^+A^- \xrightarrow{k_{\mathrm{ET}}} DA.$$

When the latter process is monitored, oscillations in the populations of the electronic states are observed. Previous efforts to understand these coherences have focused on the regime of small nonadiabatic electronic coupling between the electronic states.[7–9] Complicated decay of the acceptor electronic state population is calculated on time scales from 100 fs to a couple of picoseconds in model polar solvents.[10,11] Previous theoretical treatment of electron transfer in mixed valence systems has also been limited to the small coupling regime. In this regime, a nonequilibrium golden rule (GR)[7] formula can be derived to calculate the electronic state populations on the donor and acceptor electronic surfaces. This formula, a generalization of the usual GR relaxation rate, extends its applicability to electron transfer processes where the initial nuclear state is not a rovibrational eigenstate of the modes associated with the initial electronic surface or an equilibrium distribution of such states.

Extensive experimental studies using pulsed pump–probe techniques, electronic absorption spectroscopy, and resonance Raman data have yielded a wealth of data on the mixed valence electron transfer systems.[2] Experiments are typically conducted at $\approx 200-300$ K. Results of these experiments provide information vital to modeling the electron transfer process: the strength of the nonadiabatic coupling, solvent reorganization energies and frequencies, and displacements of intramolecular vibrational modes. In fact, these experimental studies have revealed the nonadiabatic coupling constant H_{DA} to be in the region of $1000-3000\ \mathrm{cm}^{-1}$. In this regime, the applicability of the

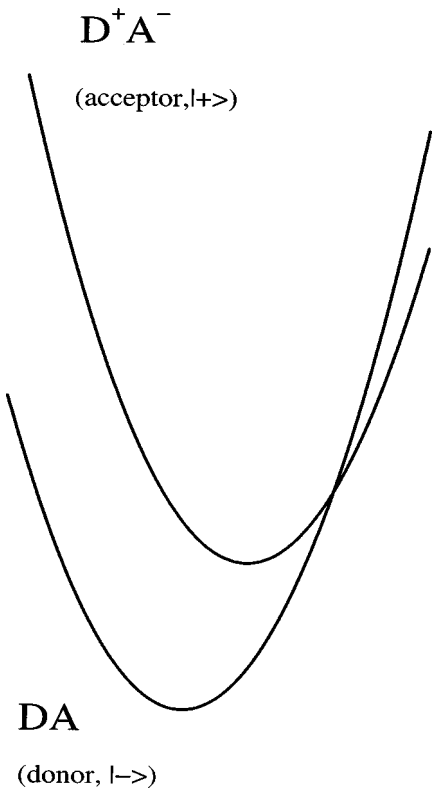

FIG. 1. Schematic of the diabatic potential surfaces for the photoexcited electron transfer reaction of $(NH_3)_5Fe^{II}(CN)(Ru)^{III}(CN)_5$.

golden rule, and the nonequilibrium golden rule formula, is highly questionable.

Our aim here is to examine the evolution of the photoexcited state, to clarify the source of the observed oscillations, and to test the validity of the GR. To this end, exact path integral calculations are performed on a mixed valence system: Experimental data[1] from the aqueous solutions of $(NH_3)_5Fe^{II}(CN)(Ru)^{III}(CN)_5$ is used to fit the effects of the vibrational degrees of freedom of the solvent to an effective harmonic bath. Understanding the time evolution also requires a detailed knowledge of the coupling of the intramolecular modes to the electron transfer process, and the data have already been extracted from resonance Raman experiments.[1] The transfer matrix path integral approach introduced by Makarov and Makri[12–14] is used to monitor the electron transfer reaction until nearly all population from the acceptor state has been transferred onto the donor electronic state, and to observe the long time transients associated with the process.

In Sec. II, the methodology involved in setting up a model Hamiltonian and solving the necessary equations is presented. In Sec. III, the results of our calculations are compared with experimental observables and with GR calculations. Finally in Sec. IV, the relevance of the results for interpreting the experimental findings is discussed.

II. METHODOLOGY

The frequencies and displacements of the eight most important intramolecular vibrational modes were taken directly from the resonance Raman experiments.[1] Data obtained from

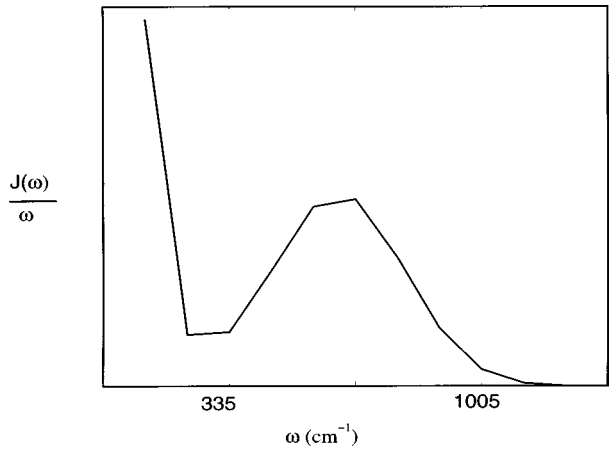

FIG. 2. The bimodal spectral density $J(\omega)/\omega$ vs ω.

the experimental electronic absorption spectrum also provide a measure of the exothermicity ΔG_0, and the solvent reorganization energy.

It is *assumed* that the solvent spectral density is Ohmic,[15] and so the distribution of solvent modes is fit to a spectral density of the form

$$J(\omega)=\eta e^{-\omega/\omega_c}, \tag{2.1}$$

where ω_c is taken as $220\ \mathrm{cm}^{-1}$ and η is adjusted to ensure that the total reorganization energy agrees with the experimental data. While the spectral density of any real liquid is expected to be much more complicated than a simple Ohmic bath,[16] this fit takes into account low frequency modes of a typical polar solvent, but of course ignores higher frequency motions. In order to check the sensitivity of our results to this fit, a bimodal spectral density was also considered. This bimodal density attempts to capture both low frequency collective motions and higher frequency librational modes, as observed in $Fe^{II/III}$–*water* molecular dynamics simulations.[17] This spectral density is illustrated in Fig. 2.

The effects on the final electron transfer rates on this choice of spectral density will be examined numerically in Sec. III. The choice of the Ohmic bath parameters was checked by calculating the electronic absorption spectrum using this harmonic bath. The calculated electronic absorption spectrum using an Ohmic bath and the internal modes is compared with the experimental absorption spectrum in Fig. 3. The observed agreement suggests that working with this model spectral density for the calculation of electron transfer in this system is reasonable.

In the GR description of electron transfer from a nonequilibrium initial state,[7] the specific question asked is: Given preparation of an initial nuclear wave packet $\phi_0(x)$ on the electronic surface $|+\rangle$, what is the probability that the electron remains on this surface at a later time t, or, equivalently, what is the time dependence of the electronic population on the electronic state $|+\rangle$, $P_+(t)$? The nonequilibrium golden rule result is (with $\hbar=1$ here, and throughout)

$$P_+^{\mathrm{GR}}(t)\cong\exp\left(-\int_0^t dt'\,k(t')\right), \tag{2.2a}$$

where

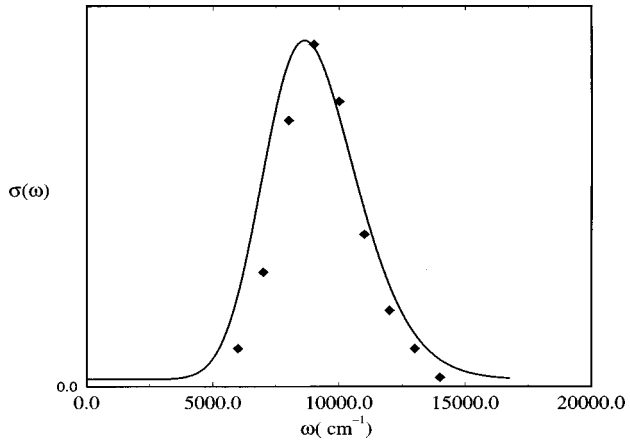

FIG. 3. Comparison of the calculated electronic absorption spectrum (diamonds) and the experimental electronic absorption spectrum (Ref. 1).

$$k(t)=2\ \mathrm{Re}\ \int_0^t dt'\langle\phi_0|e^{i\hat{h}_+t}\hat{H}_{DA}e^{-i\hat{h}_-(t-t')}\hat{H}_{DA}e^{-i\hat{h}_+t'}|\phi_0\rangle. \tag{2.2b}$$

This expression holds under a number of physical conditions, one of which is ''one-way flow,'' i.e., the probability amplitude that leaks onto the $|-\rangle$ electronic state does not find its way back to the $|+\rangle$ state. This is intuitively expected for small H_{DA} and we make the ansatz that Eq. (2.2) holds also for general nonstationary $|\phi_0\rangle$, provided that the conditions for one-way flow are satisfied.

For the high values of the nonadiabatic coupling matrix element, H_{DA}, that are observed in the experiments, it is unlikely that the golden rule will be able to describe the correct dynamics. This motivates using path integral calculations to provide an accurate time scale for the electron transfer dynamics and an interpretation of the processes involved. To this end, the electron transfer problem is approximately mapped onto the well-studied spin-boson problem,[15,18–20] where the electronic states are represented in a two-state basis. Each electronic surface has associated with it a set of nuclear degrees of freedom. As noted, these degrees of freedom are displaced harmonic modes and include both intramolecular vibrations and the softer solvent modes. It is assumed that these modes are not coupled directly to each other, but coupled only indirectly via the electronic states.

The solution of this system is nevertheless nontrivial since the large number of nuclear modes are in fact coupled indirectly to each other via the nonadiabatic coupling matrix element. The electron transfer process is modeled with the following spin-boson Hamiltonian:[11,15]

$$\hat{H}_{\mathrm{ET}}=\hat{h}_+|+\rangle\langle+|+\hat{h}_-|-\rangle\langle-|+H_{DA}(|+\rangle\langle-|+|-\rangle\langle+|). \tag{2.3}$$

For our photoinduced electron transfer process $|+\rangle$ and $|-\rangle$ are, respectively, the diabatic electronic states corresponding to the acceptor and donor electronic configurations shown in Fig. 1. The nuclear coordinate Hamiltonians $\hat{h}_\pm$ are specified as

$$h_\pm=\sum_k\left(\frac{1}{2}(p_k^2+\omega_k^2x_k^2)\pm\delta_kx_k\right)\pm\frac{\Delta G_0}{2}. \tag{2.4}$$

$\hat{H}_{\mathrm{ET}}$ may be expressed in the form of a spin-$\frac{1}{2}$ system (represented by 2×2 Pauli spin matrices σ_x and σ_z and the 2×2 unit matrix) coupled to a set of harmonic solvent coordinates $\{x_k\}$:

$$\hat{H}_{\mathrm{ET}}=\sigma_xH_{DA}+\sigma_z\sum_k\ \delta_kx_k+\sum_k\left(\frac{p_k^2}{2}+\frac{1}{2}\ \omega_k^2x_k^2\right)\mathbf{1}+\sigma_z\frac{\Delta G_0}{2}. \tag{2.5}$$

A convenient way to calculate the time evolution of the electronic state populations of the spin-boson Hamiltonian is via the path integral formalism.[21,14,19] Starting from an initial wave packet $|\phi_0\rangle$ on the $|+\rangle$ electronic surface, the probability to remain on this surface at time t is given by[21]

$$P_+(t)=\langle+|\langle\phi_0|e^{i\hat{H}_{\mathrm{ET}}t}|+\rangle\langle+|e^{-i\hat{H}_{\mathrm{ET}}t}|\phi_0\rangle|+\rangle. \tag{2.6}$$

This can be recast in the form:

$$\begin{aligned}P_+(t)=&\sum_{s_1^+=\pm1}\cdots\sum_{s_{N-1}^+=\pm1}\sum_{s_1^-=\pm1}\cdots\sum_{s_{N-1}^-=\pm1}\\&\times\langle\phi_0|\langle+|e^{i\hat{H}_{\mathrm{ET}}\epsilon}|s_{N-1}^+\rangle\langle s_{N-1}^+|\cdots|s_1^+\rangle\langle s_1^+|e^{i\hat{H}_{\mathrm{ET}}\epsilon}\\&\times|+\rangle\langle+|e^{-i\hat{H}_{\mathrm{ET}}\epsilon}|s_{N-1}^-\rangle\langle s_{N-1}^-|\ldots|s_1^-\rangle\langle s_1^-|e^{-i\hat{H}_{\mathrm{ET}}\epsilon}\\&\times|+\rangle|\phi_0\rangle,\end{aligned} \tag{2.7}$$

where $\epsilon=t/N$ and $|s_i^\pm\rangle$ is an eigenstate of σ_z, i.e., $\sigma_z|\pm1\rangle=\pm|\pm1\rangle$. Equation (2.7) is exact for any N, but practical expressions for the individual matrix elements can be given only for large N, i.e., $\epsilon\to0$. In this limit, each of the propagators may be disentangled [with errors at $\mathcal{O}(\epsilon^2)$] to give

$$\langle s_2^-|e^{-i\hat{H}_{\mathrm{ET}}\epsilon}|s_1^-\rangle\cong\mathscr{T}_{s_2^-,s_1^-}\ \exp(-i\epsilon\hat{h}_{+,-}), \tag{2.8}$$

where

$$\mathscr{T}_{s_2^-,s_1^-}=\begin{cases}\cos(\epsilon H_{DA}), & s_1^-=s_2^-\\ -i\ \sin(\epsilon H_{DA}), & s_1^-\neq s_2^-\end{cases} \tag{2.9}$$

and

$$h_{+,-}=\begin{cases}\hat{h}_+, & s_1^-=+1\\ \hat{h}_-, & s_1^-=-1,\end{cases} \tag{2.10}$$

$$\begin{aligned}P_+(t)=&\sum_{s_1^+=\pm1}\cdots\sum_{s_{N-1}^+=\pm1}\sum_{s_1^-=\pm1}\cdots\sum_{s_{N-1}^-=\pm1}\mathscr{W}_C\\&\times\exp\left[i\epsilon\left(\sum_{j=0}^{N-1}s_j^+-\sum_{k=1}^{N-1}s_k^-\right)\frac{\Delta G_0}{2}\right]\\&\times\langle\phi_0|(\hat{U}_C^b)^\dagger\hat{U}_C^f|\phi_0\rangle.\end{aligned} \tag{2.11}$$

Here $\mathscr{W}_C$ is the factor $\Pi_{j=1}^N\mathscr{T}_{s_j^+,s_{j-1}^+}\mathscr{T}_{s_j^-,s_{j-1}^-}$, and $\hat{U}_C^f$ is the time development operator for a set of linearly driven harmonic oscillators evolving according to

$$\hat{h}_k^0(x_k)+f_k^f(u)x_k.$$

Here $\hat{h}_k^0(x_k)$ is the standard harmonic oscillator Hamiltonian for mode k and u is the time variable. Furthermore, $f_k^f(u)$ is a pulse function that on the interval $j\epsilon<u<(j+1)\epsilon$ takes values of $\pm\delta_k$ if $s_j^-=\pm$ for $0\leqslant j\leqslant N-1$. The propagator $\hat{U}_C^b$ is defined analogously, and $\langle\phi_0|(\hat{U}_C^b)^\dagger\hat{U}_C^f|\phi_0\rangle$ may therefore be calculated using typical boson operator techniques.[22]

The numerical effort scales as 2^{2N} for N time slices of the total time required, and so for longer time decays, the performance of this method rapidly deteriorates. This direct calculation is therefore numerically feasible only for short-time studies of the population decay.[21] As a general rule of thumb, explicit summations will be successful only for times such that $t\ H_{DA}<10$. In the case of the mixed valence compounds, this technique will enable converged results of the electronic surface populations up to 5–10 fs. In fact, despite the large coupling, relaxation of the $|+\rangle$ electronic state occurs (somewhat surprisingly) on a considerably slower time scale, and preliminary calculations with exact spin summations could only track the $|+\rangle$ electronic population down to about 60%–70%.

In order to follow the electronic state population decay until transfer is nearly complete, we used a numerical technique that was introduced by Makri and Makarov.[12–14] Electronic surface populations are calculated using path integral methods, with electronic evolution described by local spin interactions incorporated into a transfer matrix formalism to allow for accurate long-time calculations of electron transfer in dissipative baths. This method has been successfully applied to model spin boson Hamiltonians [Eq. (2.3)] with harmonic baths having smooth spectral densities. In attempting to understand the dynamics of electron transfer in the strongly coupled mixed valence compounds, we will need to incorporate the effects of both the intramolecular modes and the fitted harmonic bath that describes the solvent modes.

The $|+\rangle$-state electronic population may be obtained from a projection of the reduced density tensor A as follows[12–14] ($\Delta k_{\max}$ denotes the maximum range for spin–spin interaction along the spin path):

$$P_+(N\Delta t)=A^{\Delta k_{\max}}(s_N^\pm=1,s_{N+1}^\pm=\cdots s_{N+\Delta k_{\max}}^\pm=0,N\Delta t). \tag{2.12}$$

In the case of equilibrium initial conditions the evolution of the reduced density tensor A can be written as

$$A^{\Delta k_{\max}}(s_{k+\Delta k_{\max}}^\pm,\ldots,s_{k+2\Delta k_{\max}-1}^\pm;[k+\Delta k_{\max})\Delta t]$$
$$=\sum_{s_k^\pm=\pm1}\cdots\sum_{s_{k+\Delta k_{\max}-1}^\pm=\pm1}T^{2\Delta k_{\max}}(s_k^\pm,\ldots,s_{k+2\Delta k_{\max}-1}^\pm)$$
$$\times A^{\Delta k_{\max}}(s_k^\pm,\ldots,s_{k+\Delta k_{\max}-1}^\pm;k\Delta t) \tag{2.13}$$

with

$$T^{2\Delta k_{\max}}(s_k^\pm,\ldots,s_{k+2\Delta k_{\max}-1})$$
$$=\prod_{n=1}^{k+\Delta k_{\max}-1}\Gamma^{\Delta k_{\max}+1}(s_n^\pm,\ldots,s_{n+\Delta k_{\max}}^\pm;k\Delta t)$$

and

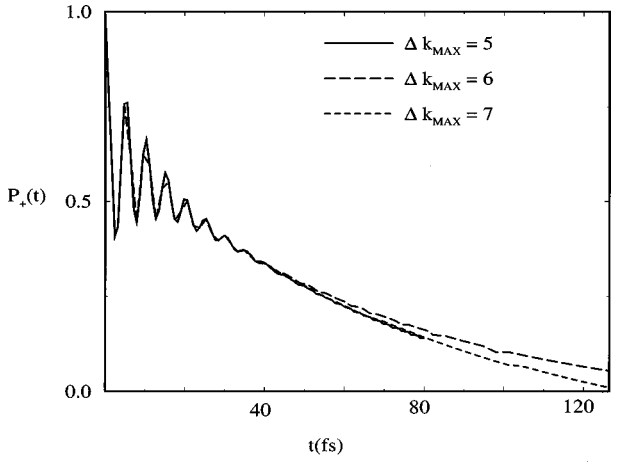

FIG. 4. The acceptor surface population $P_+(t)$ for $(NH_3)_5Fe^{II}(CN)(Ru)^{III}(CN)_5$. The results using Eq. (2.13) with $\Delta k_{\max}=5,6,7$ are indicated.

$$\Gamma^{\Delta k_{\max}+1}(s_k^\pm,\ldots,s_{k+\Delta k_{\max}}^\pm)$$
$$=K(s_k^\pm,s_{k+1}^\pm)I_0(s_k^\pm)$$
$$\times I_1(s_k^\pm,s_{k+1}^\pm)\cdots I_{\Delta k_{\max}}(s_k^\pm,s_{k+\Delta k_{\max}}^\pm),$$

where $K(s_k^\pm,s_{k+1}^\pm)$ is the propagator matrix for the bare two-level system with a coupling of H_{DA} between the two states, and $I_{\Delta k_{\max}}(s_k^\pm,s_{k+\Delta k_{\max}}^\pm)$ is the influence functional for the bath coordinates with correlations between the spins $s_k^\pm$ and $s_{k+\Delta k_{\max}}^\pm$.

In the case of nonequilibrium initial conditions, the term $I_0(s_k^\pm)$ contains an extra term $\exp[(s_k^+-s_k^-)\int d\omega\ (\omega^2/2)\ J(\omega)\delta_g(\omega)]$. Propagation of the reduced density matrix is achieved by successive tensor multiplications from the initial condition:

$$A^{\Delta k_{\max}}(s_0^\pm,s_1^\pm,\ldots,s_{\Delta k_{\max}-1}^\pm,0)=1.$$

Convergence of the results should be checked by changing the time slice length Δt, and increasing the value of $\Delta k_{\max}$, which successively considers longer range interactions in the influence functional expression.

III. RESULTS

In this section, the results for the electron transfer dynamics of $(NH_3)_5Fe^{II}(CN)(Ru)^{III}(CN)_5$ are presented for an experiment conducted in water solvent at 300 K. The nonadiabatic coupling $H_{DA}=2500\ cm^{-1}$ and $\Delta G_0=3900\ cm^{-1}$ are taken from the experimental results. The solvent modes have been fitted to an Ohmic bath [Eq. (2.1)] with a reorganization energy of $3800\ cm^{-1}$, and the frequencies and displacements of eight intramolecular modes have been taken from the fitted resonance Raman profiles.[1,2,4,5]

In Fig. 4, convergence of the Makri–Makarov[12–14] algorithm is confirmed by comparing the results obtained using three values of $\Delta k_{\max}$ in Eq. (2.13). Figure 5 compares the exact path integral calculation [Eq. (2.11), dashed line] with the converged Makri–Makarov result (full line) as well as with the golden rule result (dashed-dot line). All agree for $t<3$ fs and the path integral results agree up to $t\approx20$ fs. However, at later times, the exact spin sum does not con-

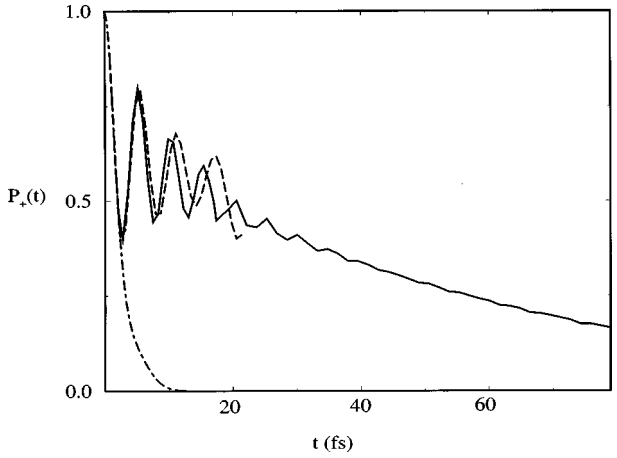

FIG. 5. The exact results [dashed line—Eq. (2.11)] and the converged approximate result [Makri–Makarov method; solid line—Eq. (2.13)] are compared with the golden rule prediction (dot-dashed line) for the aqueous solution of $(NH_3)_5Fe^{II}(CN)(Ru)^{III}(CN)_5$.

verge for the number of time slices $N \leqslant 14$. The Makri–Makarov scheme converged only for $\Delta k_{\max} \geqslant 5$ in Eq. (2.13). This large value of $\Delta k_{\max}$ is due to the presence of a discrete set of quantum modes. The local approximation would be expected to give the fastest convergence for a dense bath at high temperatures. The presence of discrete quantum modes gives rise to some small discrepancies, even at $\Delta k_{\max}=7$, due to the correlations introduced by these modes.

In Fig. 6(a), the profile of the same electron transfer event is displayed in three different situations: the first case is a frozen isolated molecule (no intramolecular vibrations). The second is an isolated molecule (in the absence of the solvent) where intramolecular vibrations are included and the third case illustrates the full model including both intramolecular vibrations and solvent modes. The solvent modes are clearly essential to understanding the electronic population decay, and this is particularly true for the long time decay tail. The intramolecular modes are, however, dominant at early times. Notice how the frequency of the early time oscillations is unchanged from the isolated molecule to the solvated state. This is consistent with our picture that these short-time oscillations are coherent oscillations between the acceptor and donor states induced by the high nonadiabatic electronic coupling.

In Fig. 6(b), the results using an Ohmic solvent of the spectral density [Eq. (2.1)] are compared with the case where the solvent modes have been fitted to the bimodal spectral density shown in Fig. 2, which captures the high and low frequency contributions found in the simulation results of Bader and Chandler.[17] The effect of different spectral densities is therefore small, if the total reorganization energy is fixed and a reasonable mean value for the solvent frequency is taken.

As indicated in Sec. I, one motivation for performing the path integral calculations is to assess the accuracy of the golden rule approximation. It is interesting to note that the golden rule predicts decay on a much shorter time scale. In Fig. 7, the nonadiabatic coupling has been decreased successively to a point where the golden rule and exact calculations

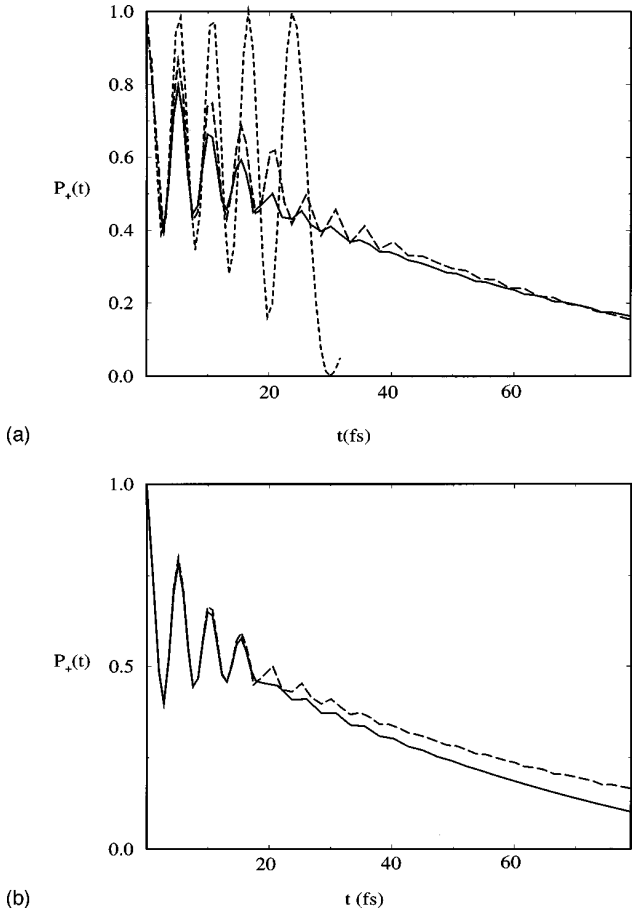

FIG. 6. (a) The effects of the nuclear modes are demonstrated. The model including both solvent and quantum modes (solid line) is compared with the model with only quantum modes (long dashed) and the model with no modes (dashed line). (b) The model using the Ohmic density, Eq. (2.1) (solid) is compared with the density in Fig. 2 (dashed line).

are in good agreement for times below 20 fs. One important result is the fact that the large electronic coupling actually gives rise to short-time coherent oscillations (not described by the golden rule) followed by a long time relaxation much slower than predicted by the golden rule result.

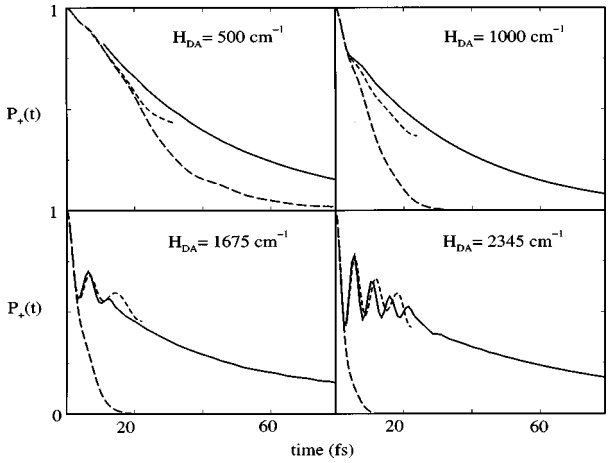

FIG. 7. The exact results using Eq. (2.11) (dashed line) are compared with the results using Eq. (2.13) (solid) and the golden rule prediction using Eq. (2.2) (long dashed line) for various strengths of the nonadiabatic coupling H_{DA}.

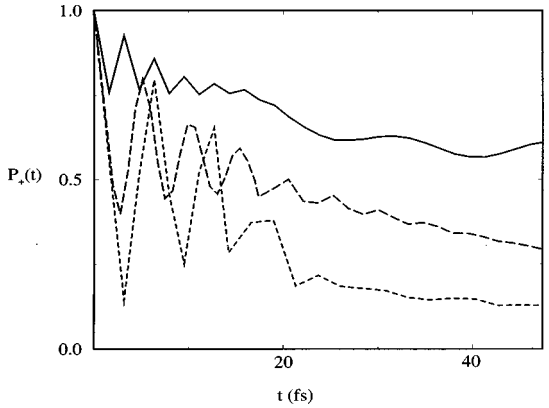

FIG. 8. The effects of initial state preparation are demonstrated here. (a) The bath is initially in an eigenstate of the donor surface (dashed line). (b) The bath is initially in an eigenstate of the acceptor surface (solid line). (c) The bath is in equilibrium when it is uncoupled from the two-state system (undisplaced oscillators) (long dashed line).

In Fig. 8, the effects of nonequilibrium initial state preparation are shown. The nonequilibrium initial state condition corresponding to the long-dashed line in Fig. 8 is probably the closest to the experimental situation in the photoexcited back electron transfer process. Pulse excitation from the equilibrated ground state gives rise to an excited electronic state where neither the intramolecular vibrations nor the solvent modes are in their equilibrium configuration. The electron transfer process that is monitored is in fact that back electron transfer following the photoexcitation to the acceptor state, during which time at least three physically relevent processes take place: change in electronic population, intramolecular nuclear rearrangement, and solvent reorganization. From Figs. 6 and 8, three things should be noted: first, the fast oscillations between the strongly coupled electronic surfaces, second, the population decay to equilibrium on a much slower time scale, and third, the fact that the electron transfer reaction is basically complete after about 90 fs.

IV. DISCUSSION AND CONCLUSIONS

Understanding the results of femtosecond experiments on electron transfer processes in the condensed phase is greatly facilitated by knowing the time scales of the various physical processes that follow the initial excitation pulse. In back electron transfer reactions, these processes include both electronic state population relaxation and reorganization of both solvent and intramolecular modes. In a set of recent experiments on charge transfer in mixed valence compounds, the short-time transient absorption spectra show complex oscillations on the subpicosecond time scale.[1,2,4,5]

To understand electron transfer processes from nonequilibrium initial conditions of the nuclear modes, we had previously made use of a generalization of the golden rule formula to initial nuclear states which are not rovibrational eigenstates of the nuclear Hamiltonian associated with the excited (acceptor) electronic surface. These studies had shown oscillations in the electronic state population, due to oscillations of the vibrational wave packet motion.

In this work we have focused directly on the experimental data of $(NH_3)_5Fe^{II}(CN)(Ru)^{III}(CN)_5$ in aqueous solvent. This system has been well studied experimentally: Resonance Raman experiments have provided details of the intramolecular modes, the solvent reorganization energy and electron absorption spectra have provided the exothermicity of the electron transfer reaction. The nonadiabatic coupling parameter H_{DA} deduced from intervalence band intensity is $2500\ cm^{-1}$ (Ref. 23) using an extended Mulliken–Hush analysis[24] for the high coupling regime. Our aim has been to compute the electron transfer dynamics of this system using path integral methods and compare the results to other methods that use the golden rule. This has been motivated by our suspicion that for the large H_{DA} and fast experimentally measured nonadiabatic transition rates, the golden rule may be inappropriate.

Our results have not only confirmed this inadequacy, but have also provided a detailed study of the electron transfer process. The large electronic coupling actually gives rise to coherent electronic population oscillations between the donor and acceptor states at very short times (<10 fs), followed by a slower relaxation on a much longer time scale (90 fs). We have found that direct spin path summation of the path integral solution to the model electron transfer Hamiltonian is not able to provide converged data for this longer time relaxation process, but the transfer matrix algorithm of Makri and Makarov yielded converged results. The experimentally deduced time for the ground-state recovery in the $(NH_3)_5Fe^{II}(CN)(Ru)^{III}(CN)_5$ system is roughly 90 fs, in gratifying (and partly fortuitous) agreement with the simulations, as is the time scale ($\leqslant 20$ fs) of the electronic coherences predicted from the experimental data.[2]

Figure 7 shows that the very short time decay ''is captured'' by the golden rule for all investigated values of H_{DA}. To be more precise, the very short time decay is purely electronic and

$$P_+(t)=\frac{\Delta G_0^2}{\Delta G_0^2+H_{DA}^2}+\frac{H_{DA}^2}{\Delta G_0^2+H_{DA}^2}\cos^2\left(\sqrt{\Delta G_0^2+H_{DA}^2}\,t\right).$$

This behavior is shown at very short times, and it must hold at short enough times, but it is probably not observable. Nevertheless, the inadequacy of the golden rule lies in the prediction of the long-time behavior and the observed electron transfer rate that results from the failure of the ''one-way flow'' assumption discussed in Sec. II: for large H_{DA}, the density can oscillate back to the $|+\rangle$ state (having initially decayed onto the $|-\rangle$ state) before energy transfer to the vibrations (of both the solvent and intramolecular modes) or intramolecular vibrational relaxation (which is actually absent in the spin-boson model) can occur. This causes oscillations (Figs. 4–8) in the diabatic state population $P_+(t)$. As is clear from Fig. 6(a), these oscillations are indeed dominated by the electronic terms ΔG_0 and H_{DA}.

Although many parameters of the particular experimental system are known in rich detail, the exact frequencies and displacements of the the solvent (water) modes are not

known. This is a shortcoming in the modeling process, although our study has shown that a number of reasonably chosen smooth spectral densities give agreement with the electronic absorption spectrum, and have relatively small effect on the electron transfer dynamics.

These results demonstrate that the oscillations observed on the picosecond time scale in the experiments cannot be attributed to coherences in the electron transfer event, since almost all the electronic population has been transferred before 90 fs. Further dynamics studies involving simulations of the relaxing solvent modes may provide an answer to the mechanism for generating these signatures in the transient absorption spectra. It is likely that these oscillations are a consequence of solvent reorganization, but obviously more detailed molecular dynamics simulations are required. In particular, further studies are needed to address the observed isotope effect on both the fast electron transfer rates and the longer timescale processes.[5] This is obviously not dealt with in these studies and is a topic for further research.

ACKNOWLEDGMENTS

We would like to thank Professor J. T. Hupp and Professor P. F. Barbara for many useful conversations and insights. M.A.R. acknowledges the support of the Chemistry division of the NSF, A.N. acknowledges the support of of the Israel Science Foundation and the Israel Ministry of Science, and D.G.E. the support of a SURP grant from Sandia National Laboratory and generous computer support from the Albuquerque High Performance Computing Center (AHPCC).

[1] H. Lu, V. Petrov, and J. T. Hupp, Chem. Phys. Lett. **235**, 521 (1995); L. Karki, H. P. Lu, and J. T. Hupp, J. Phys. Chem. **100**, 15637 (1996); H. Lu, J. N. Prieskorn, and J. T. Hupp, J. Am. Chem. Soc. **115**, 4927 (1993).

[2] P. J. Reid, C. Silva, P. F. Barbara, L. Karki, and J. T. Hupp, J. Chem. Phys. **99**, 2609 (1995).

[3] (a) U. Banin and S. Ruhman, J. Chem. Phys. **99**, 4391 (1992); (b) K. Wynne, G. D. Reid, and R. M. Hochstrasser, *ibid.* **105**, 2287 (1996); (c) Q. Wang, R. W. Schonlein, L. A. Peterov, R. A. Mathies, and C. V. Schank, Science **266**, 422 (1994); (d) L. Zhu, J. T. Sage, and R. M. Champion, *ibid.* **266**, 679 (1994); (e) L. D. Ziegler, R. Fan, A. R. Desrosiers, and N. F. Scherer, J. Chem. Phys. **100**, 1823 (1994); (f) D. Jonas, S. Bradford, S. Passino, and G. Fleming, J. Phys. Chem. **99**, 2554 (1995); (g) P. F. Barbara, T. J. Meyer, and M. A. Ratner, *ibid.* **100**, 13148 (1996).

[4] (a) G. C. Walker, P. F. Barbara, S. K. Doorn, Y. Dong, and J. T. Hupp, J. Phys. Chem. **95**, 5712 (1991); (b) P. F. Barbara, G. C. Walker, and T. P. Smith, Science **256**, 975 (1992); (c) G. C. Walker, E. Akesson, A. E. Johnson, N. E. Levinger, and P. F. Barbara, J. Phys. Chem. **96**, 3728 (1992).

[5] (a) K. Tominaga, D. A. V. Kliner, A. E. Johnson, N. E. Levinger, and P. F. Barbara, J. Chem. Phys. **99**, 2613 (1995); (b) P. J. Reid, C. Silva, Y. Dong, J. T. Hupp, and P. F. Barbara, Ninth International Conference on Ultrafast Phenomena, 1993 (unpublished); (c) K. Tominaga, D. A. V. Kliner, A. E. Johnson, N. E. Levinger, and P. F. Barbara, J. Chem. Phys. **98**, 1228 (1993).

[6] (a) M. Bixon and J. Jortner, J. Chem. Phys. (in press); (b) J. M. Jean, *ibid.* **104**, 5638, (1996); (c) L. Seidner, G. Stock, and W. Domcke, *ibid.* **103**, 3598 (1995).

[7] R. D. Coalson, D. G. Evans, and A. Nitzan, J. Chem. Phys. **101**, 486 (1994).

[8] E. Neria and A. Nitzan, J. Chem. Phys. **99**, 1109 (1993); Chem. Phys. Lett. **183**, 351 (1994).

[9] M. D. Todd, A. Nitzan, and M. A. Ratner, J. Phys. Chem. **97**, 29 (1993).

[10] D. G. Evans and R. D. Coalson, J. Chem. Phys. **104**, 3598 (1996).

[11] D. G. Evans and R. D. Coalson, J. Chem. Phys. **102**, 5658 (1995).

[12] D. E. Makarov and N. Makri, Chem. Phys. Lett. **221**, 482 (1994).

[13] N. Makri and D. E. Makarov, J. Chem. Phys. **102**, 4600 (1995); **102**, 4611 (1995).

[14] N. Makri, J. Math. Phys. **36**, 2430 (1995).

[15] (a) A. J. Leggett, S. Chakravarty, A. T. Dorsey, M. P. A. Fisher, A. Garg, and W. Zwerger, Rev. Mod. Phys. **59**, 1 (1987); (b) A. O. Caldeira and A. J. Leggett, Ann. Phys. (N.Y.) **149**, 374 (1983).

[16] N. F. Scherer, J. Chem. Phys. **99**, 4391 (1992).

[17] J. Bader and D. Chandler, J. Chem. Phys. **99**, 4391 (1992).

[18] A. Garg, J. N. Onuchic, and V. Ambegaokar, J. Chem. Phys. **83**, 4491 (1985); see also, J. N. Onuchic, *ibid.* **86**, 3925 (1987); J. N. Onuchic, D. N. Beratan, and J. J. Hopfield, J. Phys. Chem. **90**, 3707 (1986).

[19] (a) J. Cao and G. Voth, J. Chem. Phys. **105**, 6586 (1997); (b) **106**, 1769 (1997); (c) C. Mak, *ibid.* **99**, 4391 (1992); (d) J. T. Stockburger and C. H. Mak, *ibid.* **105**, 8126 (1996); (e) R. Egger and C. H. Mak, Phys. Rev. B **50**, 15210 (1994); (f) P. Hanggi, J. Chem. Phys. **99**, 4391 (1992); (g) P. Hanggi, *ibid.* **99**, 4391 (1992).

[20] (a) M. Winterstetter and W. Domcke, Chem. Phys. Lett. **236**, 445 (1995); (b) M. Winterstetter and U. Weiss, Chem. Phys. **209**, 1 (1994); (c) S. Krempl, M. Winterstetter, and W. Domcke, J. Chem. Phys. **102**, 6499 (1995); (d) S. Krempl, M. Winterstetter, and H. Plohn, *ibid.* **100**, 926 (1993).

[21] (a) R. D. Coalson, J. Chem. Phys. **86**, 995 (1987); (b) Phys. Rev. B **39**, 12502 (1989); (c) J. Chem. Phys. **94**, 1108 (1991).

[22] See, for example, P. Pechukas and J. C. Light, J. Chem. Phys. **44**, 3897 (1965).

[23] Private communication with J. T. Hupp.

[24] (a) L. Karki, H. Lu, and J. Hupp, J. Phys. Chem. **100**, 15637 (1996); (b) C. Creutz, M. Newton, and N. Sutin, J. Photochem. Photobiol., B **82**, 47 (1994); (c) R. Cave and M. D. Newton, Chem. Phys. Lett. **249**, 15 (1996).